



HAL
open science

A sparse EEG-informed fMRI model for hybrid EEG-fMRI neurofeedback prediction

Claire Cury, Pierre Maurel, Rémi Gribonval, Christian Barillot

► To cite this version:

Claire Cury, Pierre Maurel, Rémi Gribonval, Christian Barillot. A sparse EEG-informed fMRI model for hybrid EEG-fMRI neurofeedback prediction. 2019. inserm-02090676v2

HAL Id: inserm-02090676

<https://inserm.hal.science/inserm-02090676v2>

Preprint submitted on 16 Jul 2019 (v2), last revised 1 Jan 2020 (v3)

HAL is a multi-disciplinary open access archive for the deposit and dissemination of scientific research documents, whether they are published or not. The documents may come from teaching and research institutions in France or abroad, or from public or private research centers.

L'archive ouverte pluridisciplinaire **HAL**, est destinée au dépôt et à la diffusion de documents scientifiques de niveau recherche, publiés ou non, émanant des établissements d'enseignement et de recherche français ou étrangers, des laboratoires publics ou privés.

A sparse EEG-informed fMRI model for hybrid EEG-fMRI neurofeedback prediction

Claire Cury^{1,2,*}, Pierre Maurel¹, Rémi Gribonval² and Christian Barillot¹

¹Univ Rennes, CNRS, Inria, Inserm, IRISA UMR 6074, Empenn team ERL U 1228, F-35000 Rennes, France.

²Univ Rennes, CNRS, Inria, IRISA UMR 6074, PANAMA team, F-35000 Rennes, France.

Correspondence*:

Claire Cury

claire.cury.pro@gmail.com

ABSTRACT

Measures of brain activity through functional magnetic resonance imaging (fMRI) or Electroencephalography (EEG), two complementary modalities, are ground solutions in the context of neuro-feedback (NF) mechanisms for brain rehabilitation protocols. While NF-EEG (real-time neurofeedback scores computed from EEG signals) have been explored for a very long time, NF-fMRI (real-time neurofeedback scores computed from fMRI signals) appeared more recently and provides more robust results and more specific brain training. Using simultaneously fMRI and EEG for bi-modal neurofeedback sessions (NF-EEG-fMRI, real-time neurofeedback scores computed from fMRI and EEG) is very promising to devise brain rehabilitation protocols. However, fMRI is cumbersome and more exhausting for patients. The original contribution of this paper concerns the prediction of bi-modal NF scores from EEG recordings only, using a training phase where EEG signals as well as the NF-EEG and NF-fMRI scores are available. We propose a sparse regression model able to exploit EEG only to predict NF-fMRI or NF-EEG-fMRI in motor imagery tasks. We compare different NF-predictors stemming from the proposed model. We show that a proposed NF-predictor significantly improves the quality of NF session, over what EEG can provide alone, and correlates at 0.74 in median with the ground-truth.

Keywords: Optimisation, EEG, sparsity, machine learning, Neurofeedback, EEG-fMRI, sparsity

1 INTRODUCTION

Neurofeedback approaches (NF) provide real-time feedback to a subject about its brain activity and help him or her perform a given task (Hammond, 2011; Sulzer et al., 2013). Brain activity features are extracted, online, from a non-invasive modality (EEG or fMRI for example).

NF appears to be an interesting approach for clinical purposes, for example in the context of rehabilitation and psychiatric disorders (Sulzer et al., 2013; Birbaumer et al., 2009; Wang et al., 2017).

Functional magnetic resonance imaging (fMRI) and electro-encephalography (EEG) are the most used noninvasive functional brain imaging modalities in neurofeedback.

EEG measures the electrical activity of the brain through electrodes located on the scalp. EEG has an excellent temporal resolution (milliseconds), but a limited spatial resolution (centimeters) implying a lack of specificity. Furthermore, source localisation in EEG is a well-known ill-posed inverse problem (Grech et al., 2008).

On the other hand, blood oxygenation level dependent (BOLD) fMRI, measures a delayed hemodynamic response to neural activity with a good spatial resolution, and a temporal resolution of 1 or 2 seconds depending on the sequence used. Therefore fMRI is more specific than EEG, making the fMRI an adequate modality for neurofeedback (NF-fMRI) (Thibault et al., 2018). However the use of the MRI scanner is exhausting for patients and time consuming (NF-EEG session can be done in the patient room), hence NF-fMRI sessions cannot be repeated too many times for the same subject or patient.

During the past few years, the use of simultaneous EEG-fMRI recording has been used to understand the links between EEG and fMRI in different states of the brain activity and received recognition as a promising multi-modal measurement of the brain activity (Perronnet et al., 2018; Abreu et al., 2018). However this bi-modal acquisition is not comfortable for subjects or patients, due to the use of the fMRI scanner. The methodology to extract information from fMRI with EEG have been also intensively investigated (some methods involved in the process are reviewed here (Abreu et al., 2018)). Indeed, both modalities are sensitive to different aspect of brain activity, with different speeds. EEG provides in real time a direct measure of the changes in electrical potential occurring in the brain, while fMRI indirectly estimates brain activity by measuring changes in BOLD signal reflecting neuro-vascular activity, which occurs in general few seconds after a neural event (Friston et al., 1994; Logothetis et al., 2001). Several studies have investigated correlations between EEG signal and BOLD activity, in specific and simple tasks (de Munck et al., 2007; Goncalves et al., 2008; Engell et al., 2012; Magri et al., 2012; Scheeringa et al., 2011). Some early studies reported negative correlation between the BOLD signal in the occipital lobe and the power of alpha rhythm (7-13Hz) in occipital electrodes during eyes open - eyes closed

tasks (de Munck et al., 2007; Goncalves et al., 2008). Some studies (as (Siero et al., 2013)), have shown that in different brain areas and under different conditions, the electrophysiological and BOLD source locations match well. More recent works show different links between EEG and BOLD signals; for example in (Scheeringa et al., 2011) authors determine that alpha/beta and gamma band neural dynamics, independently contribute to the BOLD signal, whereas in (Magri et al., 2012), they suggest that the amplitude of the BOLD signal reflects the relationship between alpha and gamma band power. All those studies reveal the existence of a link between EEG and fMRI, but this relationship varies with the task, the location in the brain and the considered frequency bands.

In the literature, the term EEG-informed fMRI refers to methods extracting features from EEG signals in order to derive a predictor of the associated BOLD signal in the region of interest under study. A recent review (Abreu et al., 2018) gives a good overview of the principal EEG-informed fMRI methods and their limitations. Different strategies have been investigated, depending on the type of activity under study (epilepsy, resting state, open/closed eyes, relaxation): either by selecting one channel on interest, either by using multiple channels, before extracting features of interest. For example in (Leite et al., 2013; Formaggio et al., 2011), authors used a temporal independent component analysis to select the channel reflecting the best the epileptic seizures. In (Schwab et al., 2015), authors used a spatial, spectral and temporal decomposition of the EEG signals to map EEG on BOLD signal changes in the thalamus. From a more symmetrical way, we proposed in (Noorzadeh et al., 2017), a method for the estimation of brain source activation, improving its spatio-temporal resolution, compared to EEG or BOLD fMRI only.

However, in the context of neurofeedback, using simultaneous recording of EEG-fMRI to estimate neurofeedback scores computed in real time from features of both modalities (NF-EEG-fMRI) is a recent application that have been first introduced, and its feasibility demonstrated by (Zotев et al., 2014; Perronnet et al., 2017; Mano et al., 2017). The recent methodology synchronising both signals for real time neurofeedback (Mano et al., 2017), allows the acquisition of a new kind of data named NF-EEG-fMRI data, such as the one used here, and first presented in (Perronnet et al., 2017). Furthermore, it has been shown in (Perronnet et al., 2017), that the quality of neurofeedback session is improved when using simultaneously both modalities, in NF-EEG-fMRI sessions. Thus, being able to reproduce in real time a NF-EEG-fMRI session when using EEG only, would reduce the use of fMRI in neurofeedback, while increasing the quality of NF sessions. To export NF-fMRI scores outside the scanner, most of the methods intend to predict the fMRI BOLD signal activity on a specific region of interest by learning from EEG signal recorded simultaneously, inside the fMRI scanner. Indeed, the method proposed in (Meir-Hasson et al., 2014), uses a ridge regression model with a ℓ_2 regularisation, based on a time/frequency/delay

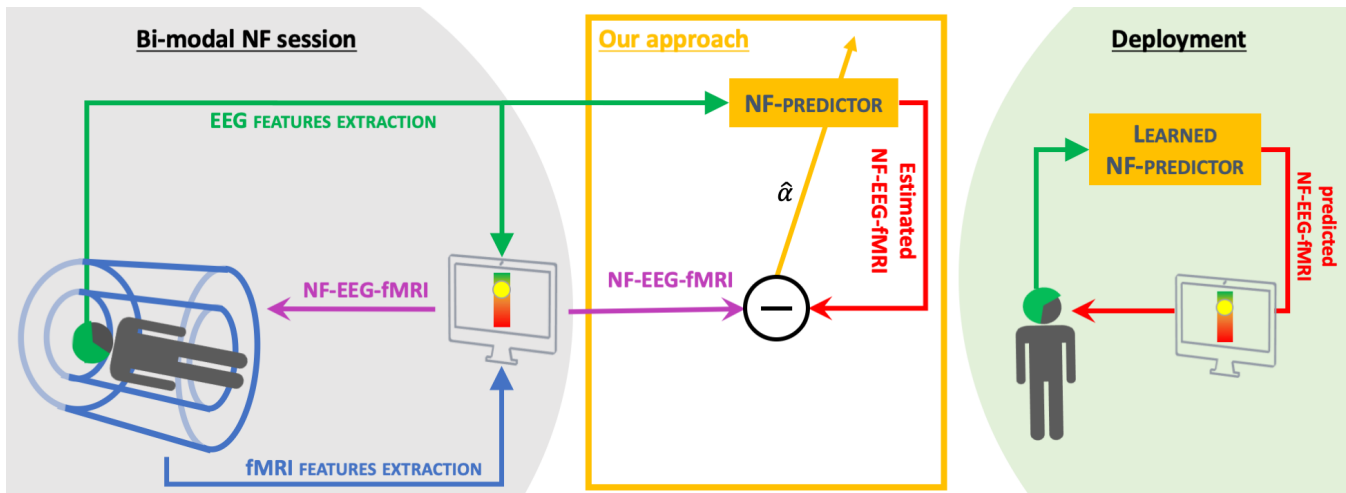


Figure 1. Objectif : From bi-modal neurofeedback sessions (NF-EEG-fMRI) (see (Perronnet et al., 2017) or section 3 for more details), we propose a method to learn a NF-predictor. The final goal of this method is to propose NF sessions using EEG only, with the quality of bi-modal NF sessions. Therefore reducing the use of fMRI.

representation of the EEG signal from a single channel. Results show a good estimation of the BOLD signal in the region of interest, but the use of the neurofeedback in this study is only to serve the paradigm.

Our challenge here, is to learn EEG activation patterns (see section 2.2) from hybrid NF-EEG-fMRI sessions (Perronnet et al., 2017), to improve the quality of neurofeedback scores when EEG is used alone. The motivation of this is multiple: since we are considering a new kind of data, we want to provide a simple method characterising NF-EEG-fMRI in EEG, leading to understandable model to confirm existing relations between EEG and fMRI in neurofeedback scores, or to discover new relationships. Neurofeedback features in fMRI come from the BOLD activation in one or more region of interest. We propose an original alternative to source reconstruction in the context of neurofeedback. Indeed we directly intent to predict NF scores, without dealing with source reconstruction or spatial filtering to estimate BOLD-fMRI signal first on a specific region of interest, as proposed by a previous approach (Noorzadeh et al., 2017). To our knowledge, this problem of prediction of hybrid neurofeedback scores (without source reconstruction) is new, and has not yet been explored in the literature. Also we want the activation pattern to be applicable in real-time when using new EEG data. The main objective of this paper (Figure 1) is to design a method able to exploit EEG only, and predict an NF score of quality comparable to the NF score that could be achieved with a simultaneous NF-EEG-fMRI session. The approach is based on a machine learning mechanism. During a training phase, both EEG and fMRI are simultaneously acquired and used to compute and synchronise, in real time, NF-EEG and NF-fMRI scores, both being combined into an hybrid NF-EEG-fMRI score (Mano et al., 2017). EEG signals and NF scores are used to learn activation patterns. During the testing phase, the learned NF-predictor (also called activation pattern) is applied to unseen EEG data, providing simulated NF-EEG-fMRI scores in

real time. Sparse regularisation is exploited to build a model called NF-predictor. The model used for the NF-predictor uses an adapted prior for brain activation patterns, using a mixed norm giving a structured sparsity, to spatially select electrodes and then select the most relevant frequency bands.

In section 2 we present the proposed model and the methods used to solve it. Then we will experiment our learning model on neurofeedback sessions with motor imagery task, which unique data are presented in section 3. Section 4 presents results on a group of 17 subjects with 3 NF sessions of motor imagery each, and compared the results to a widespread learning method, used in Brain Computing Interface to discriminate two mental states, the Common spatial pattern (CSP). Section 5 provides a discussion of the proposed framework.

2 PROBLEM AND METHOD

The approach consists in considering that, during a training phase, we have access to reference scores $y(t)$ and a temporal representation (potentially non-linear) of EEG signals \mathbf{X} (called a design matrix, presented in section 2.1), and wish to choose a parameter vector α such that $y(t) \approx q(\mathbf{X}(t), \alpha)$ for all t , where q is some parametric function. α is a matrix matching the size of $\mathbf{X}(t)$, here we consider

$$q(\mathbf{X}(t), \alpha) := \langle \mathbf{X}(t), \alpha \rangle = \sum_{i=1}^E \sum_{j=1}^F \mathbf{X}_{i,j}(t) \alpha_{i,j}. \quad (1)$$

Regularisation is used to select an optimal parameter vector $\hat{\alpha}$ that fits the training data, while avoiding over-fitting, as detailed in Section 2.2.

Only a few brain regions are expected to be activated by a given cognitive task, therefore the electrodes configuration is said to be spatially sparse. However frequency bands of each electrodes are not necessarily sparse, and might even be smooth depending on the frequency band sampling.

From here, we will use the following notations. $y_e(t) \in \mathbb{R}, \forall t \in \{1, \dots, T\}$ are the T neurofeedback scores estimated from EEG signals (noted $S_{\text{EEG}} \in \mathbb{R}^{E \times T_{\text{EEG}}}$), measured from E electrodes during T_{EEG} samples of time. $y_f(t) \in \mathbb{R}, \forall t \in \{1, \dots, T\}$ are the T neurofeedback scores extracted from Blood Oxygen Level Dependent imaging (BOLD) signal of functional-MRI acquisitions $S_{\text{fMRI}} \in \mathbb{R}^{V \times T_{\text{fMRI}}}$, with V the number of voxels and T_{fMRI} the number of acquired volumes. $y(t) \in \mathbb{R}, \forall t \in \{1, \dots, T\}$ is a set of neurofeedback scores that can be y_e , y_f or $y_c = y_e + y_f$ a combination of both (more details are provided in section 3). First, relevant information from EEG data need to be extracted and organised to form what we call a design matrix.

2.1 Structured design matrices from EEG signal

The design matrix $\mathbf{X}_0 \in \mathbb{R}^{T \times E \times B}$, where E is the number of electrodes and B the number of frequency bands, contains relevant information extracted from the EEG signal. Each temporal matrix of \mathbf{X}_0 , $\mathbf{X}_0(t) \in \mathbb{R}^{E \times B} \forall t \in \{1; \dots; T\}$ is a frequency decomposition corresponding to the past 2 seconds of S_{EEG} . We used a Hamming time window of 2 seconds, to estimate the average *power* of each frequency band $b \in \{1; \dots; B\}$ (defined below) on each channel $e \in \{1; \dots; E\}$. Each time window of EEG signal is overlapped by 1.75 seconds (0.25 seconds shift), to match with the 4Hz sample of the \mathbf{y} values. The B frequency bands have an overlap of 1 Hz with the next band, and are defined between a minimum frequency b_{\min} Hz and a maximum frequency b_{\max} Hz (see section 3). We chose to use several relatively narrow frequency bands to let the model select the relevant bands for each electrodes. Furthermore it has been suggested (de Munck et al., 2009; Rosa et al., 2010) to use different frequency bands when working with coupling EEG-fMRI data.

The model also has to be able to predict y_f scores, derived from BOLD signal (see section 3). There is no linear relationship between BOLD signal and average power on frequency bands from EEG signal. Therefore, to better match y_f scores, we decided to apply a non-linear function to \mathbf{X}_0 , used in fMRI to model BOLD signals (Pedregosa et al., 2013; Lindquist et al., 2009), the canonical Hemodynamic Response function (HRF). We convolved \mathbf{X}_0 on its temporal dimension with the HRF, formed by 2 gamma functions, for a given delay of the first gamma function to compensate the response time of BOLD signal, as suggested in (Meir-Hasson et al., 2014; Moosmann et al., 2008). The HRF will temporally smooth and give a BOLD-like shape to the design matrix and increase a potential linear relationship between y_f and design matrix. Since HRF is known to vary considerably across brain regions and subjects (Handwerker et al., 2004), it is therefore recommended to consider different delays, but also to chose a range of values corresponding to the task asked. For the type of task addressed in the experimental part, the observed delay is around 4 seconds, therefore we convolved \mathbf{X}_0 with 3 different HRF leading to 3 new design matrices $\mathbf{X}_3, \mathbf{X}_4, \mathbf{X}_5$ with respectively a delay of 3, 4 and 5 seconds for the canonical HRF.

Those design matrices are concatenated in their 2nd dimension to form the $\mathbf{X}_c \in \mathbb{R}^{T \times M \times B}$ matrix, with $M = 4 * E$. Therefore, for each time t , $\mathbf{X}_c(t) = [\mathbf{X}_0(t); \mathbf{X}_3(t); \mathbf{X}_4(t); \mathbf{X}_5(t)]$. We also denote $\mathbf{X}_d(t) = [\mathbf{X}_3(t); \mathbf{X}_4(t); \mathbf{X}_5(t)]$ the design matrix of the different delays.

2.2 Optimisation

EEG data are now represented into a structured design matrix \mathbf{X}_c , we can search for a weight matrix $\hat{\alpha} \in \mathbb{R}^{M \times B}$, such that $\sum_{m,h} \hat{\alpha}(m,h) \mathbf{X}_c(t,m,h)$ estimates as well as possible the NF score $y(t), \forall t \in \{1; \dots; T\}$. Note: the methodology is presented for the design matrix \mathbf{X}_c , but can be used for \mathbf{X}_0 or \mathbf{X}_d .

To identify the $\hat{\alpha}$, called activation pattern, we propose the following strategy, which consists in learning, for a given subject and a NF session, the optimal $\hat{\alpha}$ by solving the following problem:

$$\hat{\alpha} = \underset{\alpha}{\operatorname{argmin}} \sum_{t=1}^T \frac{1}{2} (y(t) - q(\mathbf{X}_c(t), \alpha))^2 + \phi_\lambda(\alpha) \quad (2)$$

with ϕ_λ a regularisation term, λ a weighting parameter for the regularisation term. This $\hat{\alpha}$ is then applied to a design matrix \mathbf{X}_c^{test} from a new session, to predict its NF scores

$$\tilde{y}_{\hat{\alpha}}(t) = q(\mathbf{X}_c^{test}(t), \hat{\alpha}) \quad \forall t \in \{1; \dots; T\} \quad (3)$$

Equation (2) is of the form $\operatorname{argmin}(g_1(\alpha) + g_2(\alpha))$ and its resolution can be done using the Fast Iterative Shrinkage Thresholding Algorithm (FISTA) (Beck and Teboulle, 2009), which is a two-step approach of the Forward-Backward algorithm (Combettes and Wajs, 2005) making it faster. FISTA requires the same conditions as the Forward-Backward algorithm, meaning a convex differentiable with Lipschitz gradient term g_1 and a convex term g_2 that is not necessarily differentiable but smooth enough to make its proximal map computable.

Here $g_1(\alpha) = \sum_t \frac{1}{2} (y(t) - q(\mathbf{X}_c(t), \alpha))^2$ is a sum of convex and differentiable functions with

$$\nabla g_1(\alpha) = \sum_t -\mathbf{X}_c(t)(y(t) - q(\mathbf{X}_c(t), \alpha)) \quad (4)$$

since $\forall i \in \{1; \dots; M\}, j \in \{1; \dots; B\}, [\frac{\partial q(\mathbf{X}_c(t), \alpha)}{\partial \alpha(i,j)}]_{i,j} = \mathbf{X}_c(t, i, j)$. By representing $\mathbf{X}_c(t)$ and α as vectors of size $M * B$, we can easily note that $\frac{\partial g_1}{\partial \alpha}$ is a sum of Lipschitz functions. Therefore, the Lipschitz constant of $\frac{\partial g_1}{\partial \alpha}$ is $L = \|\mathbf{X}_V^T \mathbf{X}_V\|$ with $\mathbf{X}_V \in \mathbb{R}^{T * M * B}$ the vectorised version of \mathbf{X}_c .

The NF-predictor uses structured design matrix to have a better control on the interpretation of results and to better optimise the weights $\hat{\alpha}$. Therefore we have to adopt an optimisation strategy coherent with this structure. The activation pattern of the NF-predictor:

1. has to be spatially sparse since the cognitive task is reflected by brain activity from a limited set of electrodes,

2. has to be smooth across different overlapped frequency bands,
3. has to allow non-relevant frequency bands to be null.

The term g_2 is the prior term. Here, for $g_2(\boldsymbol{\alpha}) = \phi_\lambda(\boldsymbol{\alpha})$, we chose to use a ℓ_{21} mixed norm (Ou et al., 2009) followed by a ℓ_1 -norm (noted ℓ_{21+1} -norm in (Gramfort et al., 2011)) to fit all structure conditions mentioned above.

$$\phi_\lambda(\boldsymbol{\alpha}) = \lambda \|\boldsymbol{\alpha}\|_{21} + \rho \|\boldsymbol{\alpha}\|_1 \quad (5)$$

with $\rho \in \mathbb{R}^+$ and $\lambda \in \mathbb{R}^+$. We chose not to estimate the parameter ρ , to keep computation time reasonable. Indeed, ρ weights the induced spatial sparsity over EEG channels, and we chose to fix this parameter for all subjects, as we hypothesis that there is no reason, for the number of electrodes involved in the activation pattern, to significantly change between subjects. However the estimation of λ parameter is needed (since we do not have hypothesis on its behaviour) and presented in the next section. The ℓ_{21} mixed norm that writes $\|\boldsymbol{\alpha}\|_{21} = \sum_m \sqrt{\sum_b \alpha_{m,b}^2}$ satisfies conditions 1) and 2). The ℓ_1 norm defined as $\|\boldsymbol{\alpha}\|_1 = \sum_{m,b} |\alpha_{m,b}|$ satisfies condition 3) since ℓ_p norms with $p \leq 1$ are known to promote sparsity. The last key point of FISTA algorithm is the proximal map associated to the ℓ_{21+1} norm $\text{Prox}_{\ell_{21+1}} : \mathbb{R}^{M \times B} \rightarrow \mathbb{R}^{M \times B}$, $\boldsymbol{\beta} \mapsto \text{argmin}_{\boldsymbol{\alpha}} (\phi_\lambda(\boldsymbol{\alpha}) + 1/2 \|\boldsymbol{\beta} - \boldsymbol{\alpha}\|^2)$, defined as

$$(\text{Prox}_{\ell_{21+1}}(Y))_{m,b} = \frac{Y_{m,b}}{|Y_{m,b}|} (|Y_{m,b}| - \rho)^+ \left(1 - \frac{\lambda}{\sqrt{\sum_b (|Y_{m,b}| - \rho)^{+2}}}\right)^+ \quad (6)$$

with operator $(\cdot)^+ = \max(\cdot, 0)$. One can note that by cancelling either the λ parameter or the ρ parameter, we retrieve the proximal map associated to the ℓ_{21} (when $\rho = 0$) and to the ℓ_1 norm (when $\lambda = 0$), which demonstrations can be found in the appendix of (Gramfort et al., 2012). For the stopping criterion of FISTA, a large enough number of iteration has been used, allowing the model to converge before reaching the last iteration. All elements and conditions are gathered to run the FISTA algorithm.

2.3 λ parameter selection

The parameter λ is important in the optimisation problem and we decided to estimate it automatically. The following process chooses the best λ among a list of $\Lambda = \{\lambda_1; \dots; \lambda_l\}$ sorted in increasing order. First of all, the data must be split into 2 sets. In our case subjects have 3 NF-EEG-fMRI sessions : one session is used as the learning set, and another NF-EEG-fMRI session is used as the testing set (see Figure 2). For each value λ_i of Λ , the learning set, formed by T neurofeedback scores with their associated design matrices, is divided $K = 50$ times into a training set of indices R_k , representing 90% of the T data, and a cross-validation set CV_k composed by composed by the remaining 10% of the learning set. A model

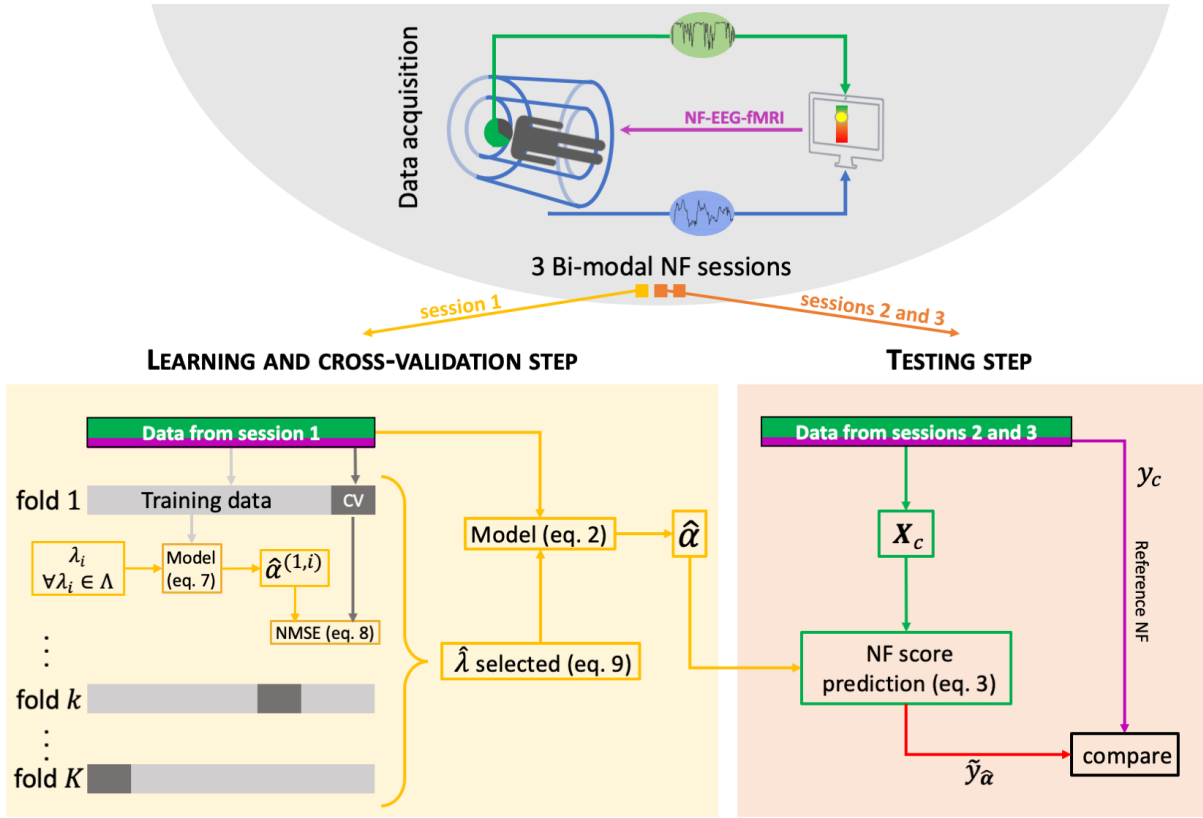


Figure 2. Machine learning scheme. For each subject, a bimodal neurofeedback session (NF-EEG-fMRI session 1 here) is used for the learning step, then the learned activation pattern $\hat{\alpha}$ is apply to the other sessions (2 and 3) for the testing step. The learning data are split K times into a training set (90% of the learning set) and a cross-validation (CV) set (10% of the learning set). The optimal $\hat{\lambda}$ parameter is the one minimising the variance and the bias in the learning step.

$\hat{\alpha}^{(k,i)}$ is estimated on the training dataset k composed by R_k neurofeedback scores $y(j)$ and the associated design matrices $\mathbf{X}_c(j)$ with λ_i , i.e.:

$$\hat{\alpha}^{(k,i)} = \arg \min \sum_j \|y(j) - q(\mathbf{X}_c(j), \hat{\alpha}^{(k,i)})\|^2 + \lambda_i \|\alpha^{(k,i)}\|_{21} + \rho \|\alpha^{(k,i)}\|_1 \quad (7)$$

with $j \in R_k$ and $\mathbf{X}_c(j) \in \mathbb{R}^{M \times B}$. For the current λ_i evaluation, we stop the process when $\sum_k |\hat{\alpha}^{(k,i)}|_0 / K < 2$. There is no need to investigate the next λ_i , the current one is sparse enough, and the next one might lead to null models.

We then apply the model $\hat{\alpha}^{(k,i)}$ to the corresponding cross-validation set of CV_k NF scores, to obtain estimated values of $y(s)$, $\tilde{y}(s) = q(\mathbf{X}_c(s), \hat{\alpha}^{(k,i)})$, with $s \in CV_k$. For each one of the 50 partitioning into training and cross-validation sets, we computed the normalised mean squared error NMSE for a given set

of data $\{y, \mathbf{X}_c\}$, for the training sets and the cross-validation sets.

$$\text{NMSE}(\{y, \mathbf{X}_c\}, \hat{\boldsymbol{\alpha}}^{(k,i)}) = \frac{\sum_s (y(s) - q(\mathbf{X}_c(s), \hat{\boldsymbol{\alpha}}^{(k,i)}))^2}{\sum_s (y(s) - \bar{y})^2} \quad (8)$$

with $\bar{y} = 1/n \sum_s y(s)$. The optimal $\hat{\lambda}$ parameter is defined as the one minimising the error during training and cross-validation. Considering only the errors from the training set $\text{NMSE}(\{y(R_k), \mathbf{X}_c(R_k)\}, \hat{\boldsymbol{\alpha}}^{(k,i)})$ would introduce bias, and considering only the error of the cross-validation set $\text{NMSE}(\{y(CV_k), \mathbf{X}_c(CV_k)\}, \hat{\boldsymbol{\alpha}}^{(k,i)})$, would introduce variance. Then the optimal $\hat{\lambda}$ is the λ_i that minimises :

$$\sum_{k=1}^K [\text{NMSE}(\{y(R_k), \mathbf{X}_c(R_k)\}, \hat{\boldsymbol{\alpha}}^{(k,i)}) + \text{NMSE}(\{y(CV_k), \mathbf{X}_c(CV_k)\}, \hat{\boldsymbol{\alpha}}^{(k,i)})] \quad (9)$$

$\hat{\lambda}$ parameter is the optimal parameter used for the model estimation. If there are several candidates, to favor sparsity, the larger of these candidate is chosen.

3 DATA ACQUISITION AND PRE-PROCESSING

We used a group of 17 subjects that were scanned using a hybrid Neurofeedback platform coupling EEG and fMRI signal (Mano et al., 2017). A 64-channel MR-compatible EEG solution from Brain Products (Brain Products GmbH, Gilching, Germany) has been used, the signal was sampled at 5kHz, FCz is the reference electrode and AFz the ground electrode. For the fMRI scanner, we used a 3T Verio Siemens scanner with a 12 channels head coil (repetition time (TR) / echo time (TE) = 2000/23ms, FOV = 210 × 210mm², voxel size = 2 × 2 × 4mm³, matrix size = 105 × 105 with 16 slices, flip angle = 90°). All subjects are healthy volunteers, right-handed and had never done any neurofeedback experiment before. They all gave written informed consent in accordance with the Declaration of Helsinki, as specified in the study presenting the data (Perronnet et al., 2017). They all had 3 NF motor imagery sessions of 320 seconds each, after a session dedicated to the calibration. One session consists in 8 blocks alternating between 20 seconds of rest, eyes open, and 20 seconds of motor imagery of their right hand. The neurofeedback display was uni-dimensional (1D) for 9 subjects (Figure 3 left), and bi-dimensional (2D) for 8 subjects (Figure 3 middle). For both, the goal was to bring the ball into the dark blue area (Perronnet et al., 2018).

NF scores y_e and y_f being from different modalities, were standardised before summing to form y_c . In this study NF scores refer to standardised scores, except when they are predicted. For this study, y_e have been computed from the commonly used, in neurofeedback, the Laplacian operator, centred around the region of interest, channel C3 here. For each time interval I_t the spatial filtering is noted $\text{Lap}(C3, I_t)$. The

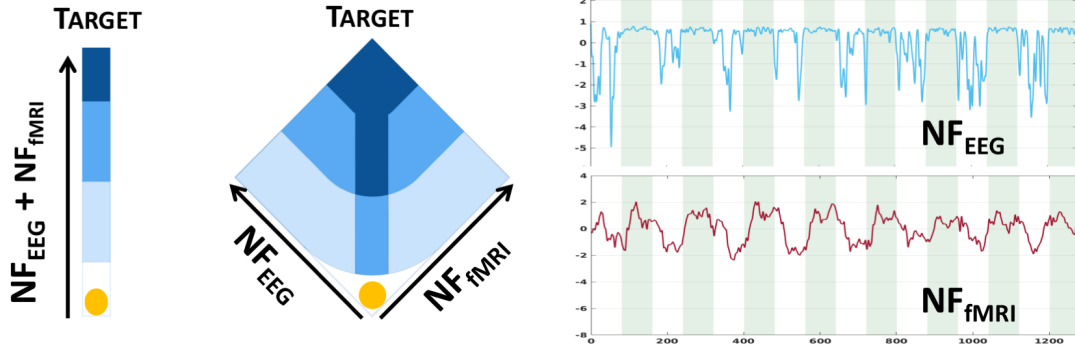


Figure 3. Bi-modal neurofeedback strategies (1D on the left, 2D on the middle), displayed during sessions (Perronnet et al., 2018). 1D: the ball’s position represents the sum of y_e and y_f . 2D: the left axis represents the y_e and the right axis represents the y_f scores. The 2 plots on the right show NF scores from EEG and from fMRI, green areas are task, white areas are rest. The goal is to bring the ball in the dark blue area.

temporal segments I_t are spaced by 250ms, and a length of 2 seconds (therefore an overlapping of 1,75 seconds), as for the design matrix construction. The power of the frequency band [8Hz - 30Hz] is then extracted via the function f :

$$y_e(t) = -f_{[8-30]}(\text{Lap}(C3, I_t))$$

One may note the presence of the minus operator used here, for the sake of coherence with y_f (Figure 3 right).

The neurofeedback scores y_f have been computed from the maximal intensity of BOLD signal covering the right-hand motor area and the supplementary motor area, one score is computed per volume acquired (i.e 1 per second). Then scores y_f are re-sampled and smoothed (using a Savitzky-Golay filter, known to avoid signal distortion) to fit the 4Hz y_e scores ($T = 1280$).

Here we introduce an other neurofeedback score, $\hat{y}_{\text{CSP}}(t) \in \mathbb{R}, \forall t \in \{1, \dots, T\}$, to be compared to our method, scores estimated from the Common Spatial Pattern (CSP) algorithm known to be efficient despite its sensitivity to noise (Ramoser et al., 2000). The CSP is a widely used filter in brain-computer interface to discriminate two mental states using EEG signals, and sometime used in the context of neurofeedback (Mano et al., 2017; Perronnet et al., 2017). Here, EEG signal are being recorded simultaneously with fMRI, the two mental states are the 20 seconds resting blocks and the 20 seconds task blocks, modulated by the neurofeedback scores y_e and y_f received by the subject. The CSP filter is used to spatially filter the EEG signal, as for the Laplacian and with the same time intervals I_t , the power of the frequency band 8-30 Hz is estimated on the filtered signal to obtain the \hat{y}_{CSP} values.

An active set have been selected on design matrices to avoid potentially correlated noise, due to head movement during resting blocks, obstructing signal from channels of interest. Indeed in coupling EEG-fMRI acquisitions, subjects are lying into the MRI scanner, therefore outer electrodes can be in contact with the bed or holds. We excluded outer electrodes and kept 28 electrodes, the 3 central lines have 7 electrodes (FCz is the reference), 3 frontal electrodes and 3 posterior electrodes.

Potential outliers in the design matrices (i.e. observations $> \text{mean} \pm 3\text{std}$) were thresholded in the NF-EEG-fMRI session used as learning set, and bad observations from annotations on the EEG signal were removed as their corresponding NF scores.

As mentioned in the previous section, for the regularisation of the NF-predictor, we used 15 values of λ_i from 100 to 3000 and fixed the parameter $\rho = 1500$.

For frequency bands of the design matrix \mathbf{X}_0 construction (cf section 2) and therefore for the other design matrices, we chose $b_{min} = 8$, $b_{max} = 30$ to cover alpha and beta frequency bands involved in motor tasks. There is $B = 10$ frequency bands, leading to bands of 3 Hz wide (with an overlap of 1Hz).

4 EXPERIMENTS AND RESULTS

As said in the previous section, we have 3 neurofeedback sessions per subjects. For each subjects, we will consider 1 session as learning set, and the 2 others as testing sets. Leading to 3 different learning sets, and 6 different testing sets per subjects.

4.1 Experiments and validation

We tested different NF-predictors for the prediction of different NF scores, $\forall t \in \{1; \dots; T\}$:

- NF-predictor 1: $\tilde{y}_{\hat{\alpha}_c}(t) = q(\mathbf{X}_c^{test}(t), \hat{\alpha}_c)$ with $\hat{\alpha}_c$ (eq. 2), learned from \mathbf{X}_c and y_c
- NF-predictor 2: $\tilde{y}_{\hat{\alpha}_e}(t) = q(\mathbf{X}_0^{test}(t), \hat{\alpha}_e)$ with $\hat{\alpha}_e$ (eq. 2), learned from \mathbf{X}_0 and y_e
- NF-predictor 3: $\tilde{y}_{\hat{\alpha}_f}(t) = q(\mathbf{X}_d^{test}(t), \hat{\alpha}_f)$ with $\mathbf{X}_d = [\mathbf{X}_3; \mathbf{X}_4; \mathbf{X}_5]$, and $\hat{\alpha}_f$ (eq. 2), learned from \mathbf{X}_d and y_f
- NF-predictor 4 : $\tilde{y}_{\hat{\alpha}_e}(t) + \tilde{y}_{\hat{\alpha}_f}(t)$ using NF-predictor 2 and NF-predictor 3
- NF-predictor 5: $y_e(t) + \tilde{y}_{\hat{\alpha}_f}(t)$ using NF-predictor 3 only

The NF-predictors 4 and 5 permit the use of the 2D score visualisation (Figure 3) to display NF scores. NF-predictor 4 is to compare to NF-predictor 1, since one directly learn the y_c , and the other cut the problem into 2 problems, NF predictors 2 and 3. NF-predictor 5 is an other alternative, in which only

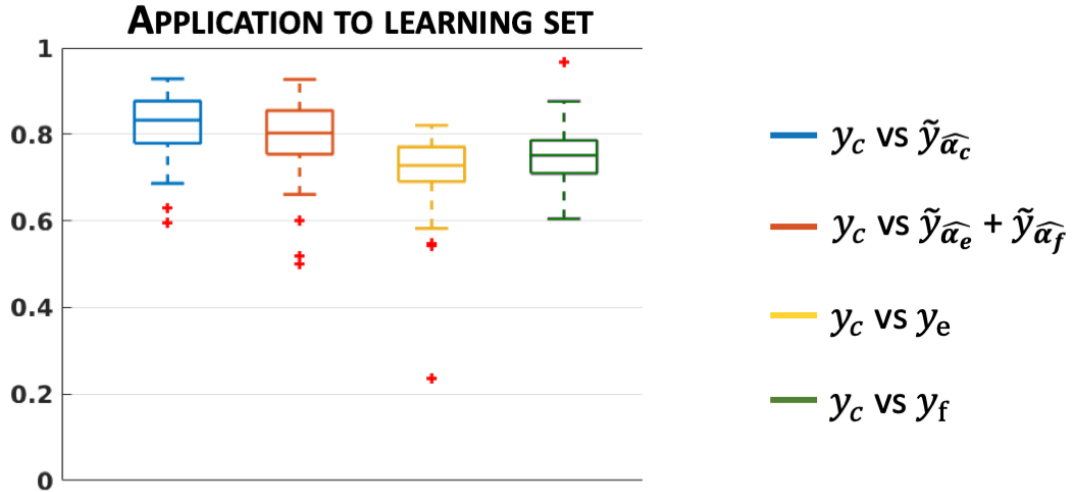


Figure 4. Model validation. Boxplots (median and quartiles) of Pearson’s correlation coefficients over all subjects and sessions, between NF-predictors and y_c , as well as between y_e and y_f with y_c .

the NF-fMRI scores are learned from EEG signal. We run the following experiments to test our different NF-predictors:

- Model validation: we used the learning set to assess if the NF-predictors could model accurately the NF scores. For each subject and each NF-predictor, we estimated correlations with the reference NF score to quantify the quality of prediction. For the validation, we compared to the correlation of y_e to y_c which is part of the y_c score, to have a correlation reference, and to know if, in the validation process, the model can do better than y_e .
- Model prediction: we apply the learned activation patterns to a new NF-EEG-fMRI session (testing set). For each subject and each pair of session (6 learning/testing pair per subject), we compared correlations between different NF-predictors to reference score y_c . We also compared the different predictions to the prediction given by the widely used, in brain computing interface and sometimes used in neurofeedback (Perronnet et al., 2017), the CSP filter (Ramoser et al., 2000), introduced in section 3.
- To observe the captured structure in the activation pattern $\hat{\alpha}_c$ learned with NF-predictor 1, we re-shaped the averaged activation patterns, over subjects and sessions, into the matrices corresponding to the design matrices defining \mathbf{X}_c (see section 2.1), and displayed results of the first dimension (electrodes) and of the second dimension (frequency bands).

4.2 Results

The model validation of the NF-predictors (i.e. the learned activation patterns $\hat{\alpha}$ are applied to the learning set) results are shown at Figure 4. Pearson’s correlation coefficients between the prediction and

Table 1. Model prediction : Median [first quartile - third quartile] of Pearson’s correlation coefficients over all subjects and sessions, between NF-predictors and y_c . The right side of the table shows p-values of left sided t-test, the hypothesis is : models in columns correlates better with y_c than models in rows.

correlation($y_{c,\cdot}$)	Med [1st q - 3rd q]	One sided paired t-test (col > row). p-values				
		NF-pred 1	NF-pred 4	NF-pred 5	y_e	\hat{y}_{CSP}
NF-predictor 1	0.50 [0.36 - 0.62]	NA	1	1	1	3e-6
NF-predictor 4	0.52 [0.38 - 0.65]	2e-3	NA	1	1	2e-7
NF-predictor 5	0.74 [0.65 - 0.79]	4e-33	3e-31	NA	0.01	1e-27
y_e	0.70 [0.64 - 0.75]	2e-19	3e-17	1	NA	4e-28
\hat{y}_{CSP}	0.36 [0.20 - 0.59]	1	1	1	1	NA

the ground truth are computed for each of the 3 learning sessions and for all subjects. The estimated $\tilde{y}_{\hat{\alpha}_c}$ (in dark blue, median $r = 0.83$, mean $r = 0.82$), on the learning set, show stronger correlation with y_c than the individual reference scores y_e (mean $r = 0.71$. paired t-test, $p \leq 1e-3$) y_f (mean $r = 0.75$. paired t-test, $p \leq 1e-3$) and $\tilde{y}_{\hat{\alpha}_e}(t) + \tilde{y}_{\hat{\alpha}_f}(t)$ (in yellow, median $r = 0.8$, mean $r = 0.79$. paired t-test, $p \leq 1e-3$). Furthermore, correlations are very high (≥ 0.8) for $\tilde{y}_{\hat{\alpha}_c}$ and $\tilde{y}_{\hat{\alpha}_e} + \tilde{y}_{\hat{\alpha}_f}$, letting think that the model is adapted to the NF prediction problem. In addition, the model could fit NF-fMRI scores using only EEG signals information with a median correlation $r = 0.80$ for $\tilde{y}_{\hat{\alpha}_f}$ vs y_f . This is promising for the proposed NF-predictor 5 which only requires the prediction of NF-fMRI scores and EEG signals only.

For the evaluation of the model prediction, the learned activation patterns are applied to the testing sets i.e. the 2 other unseen NF sessions for each one of the 3 NF sessions. Results are presented on Table 1. Table 1, shows that NF-predictor 5 (median correlation = 0.74) is the best at predicting y_c , its prediction is better than y_e only (mean correlation $y_e + \tilde{y}_{\hat{\alpha}_f}$ vs $y_c = 0.70$, mean correlation y_e vs $y_c = 0.67$). A one sided paired t-test (which alternative hypothesis is y_e has a lower correlation to y_c than $y_e + \tilde{y}_{\hat{\alpha}_f}$), gives a p-value $p = 0.01$, meaning that the prediction $\tilde{y}_{\hat{\alpha}_f}$ significantly adds information to y_e . An example of $y_e + \tilde{y}_{\hat{\alpha}_f}$ vs y_c is given in the top of Figure 5. Also NF-predictor 5 is better than any of the other model, including y_e , as shown in the second part of the table : the p-values of the one-sided paired t-test reject (highlighted row of NF-predictor 5) the hypothesis that other models better correlated with the reference score y_c . Figure 5 illustrates that, even if the correlations of $\tilde{y}_{\hat{\alpha}_c}$ (and $\tilde{y}_{\hat{\alpha}_e} + \tilde{y}_{\hat{\alpha}_f}$ too) are lower than $y_e + \tilde{y}_{\hat{\alpha}_f}$ (Table 1), $\tilde{y}_{\hat{\alpha}_c}$ can predict correctly the reference score y_c . We do not show the prediction of $\tilde{y}_{\hat{\alpha}_e} + \tilde{y}_{\hat{\alpha}_f}$, but it has the same aspect as $\tilde{y}_{\hat{\alpha}_c}$ on Figure 5.

One can note that NF-predictor 1 and NF-predictor 4 seem to be similar in term of correlation to the reference score, but the one sided t-test shows that NF-predictor 4 has a better correlation than NF-predictor 1. Predicting both y_e and y_f separately seems to be more efficient than directly predicting y_c . The correlations of NF-predictors 1 and 4 with the reference score are lower than y_e , which is expected since y_e (with all the potential noise coming from the EEG measures) is part of the reference score (as is y_e in $y_e + \tilde{y}_{\hat{\alpha}_f}$), and the regularisation of the model is smoothing the prediction of the NF-predictors.

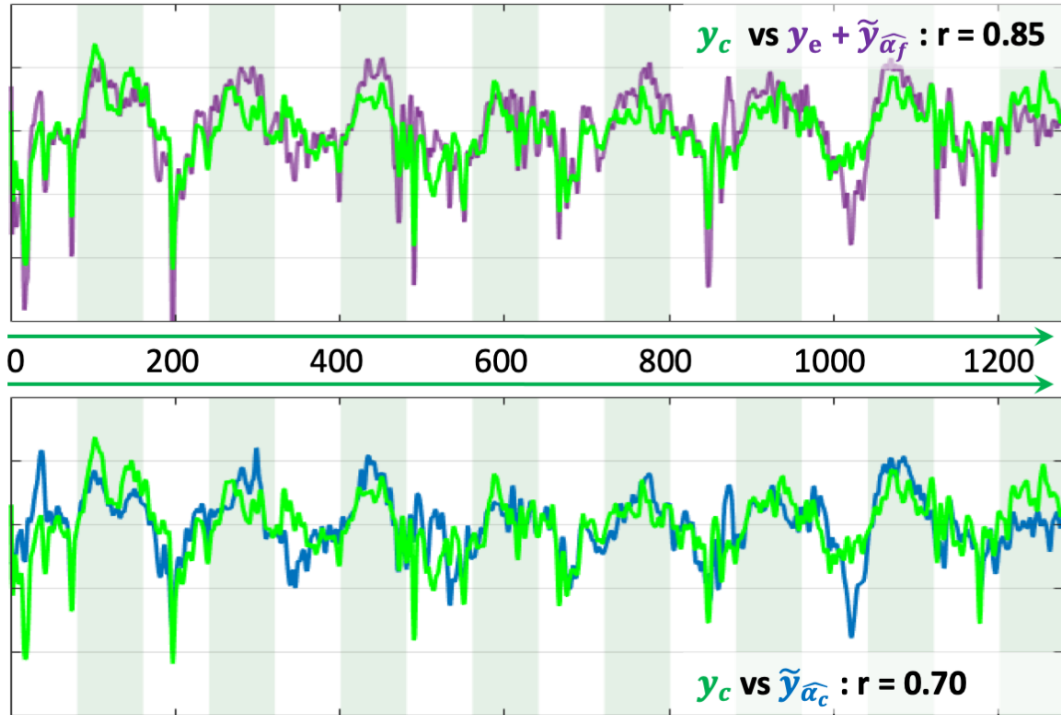


Figure 5. Examples of prediction of NF scores. Vertical bands indicate the rest and the task blocks. The correlation coefficient r indicates the correlation between each pair of time-series NF scores. The ground truth (y_c) is in green, the x-axis is the temporal axis in milliseconds. Top: NF-predictor 5 in purple. Bottom: NF-predictor 1 in blue.

At Table 1, the comparison to y_e is only here to have a point of comparison when learning phase is not done and the fMRI is not considered. The high correlation of y_e with $y_c = (y_e + y_f)$ illustrates the high frequency changes of y_e scores, which are not necessarily information.

Table 1 also shows that the predicted \hat{y}_{CSP} have the lowest correlation with the reference scores y_c , the correlations \hat{y}_{CSP} vs y_c are significantly lower than the correlation of any of the proposed NF-predictor with y_c . This is highlighted by the one sided paired t-tests (alternative hypothesis being \hat{y}_{CSP} has a lower correlation to y_c than the considered NF-predictor) which p-values are given in the last column of the second part of the table. The fact that the CSP classifier, which discriminates 2 mental states, cannot correctly predict the scores of a subject on a test session, confirms that considered signals are very noisy. Subjects can sometimes be more receptive to the EEG and sometimes to the BOLD signal, and those changes are only captured by the different neurofeedback scores obtained during the learning phase. Also subjects might adapt their strategy between sessions.

During the learning session (i.e. the NF session used to learn the predictor), if a subject focused more on NF-fMRI (which is the easiest one to control) than on NF-EEG, the EEG-signals might lose coherence with respect to the NF-fMRI scores. Even though, the EEG signals could predict NF-fMRI scores with a correlation of 0.32 in median and mean 0.3, which is a fair correlation between such different modalities.

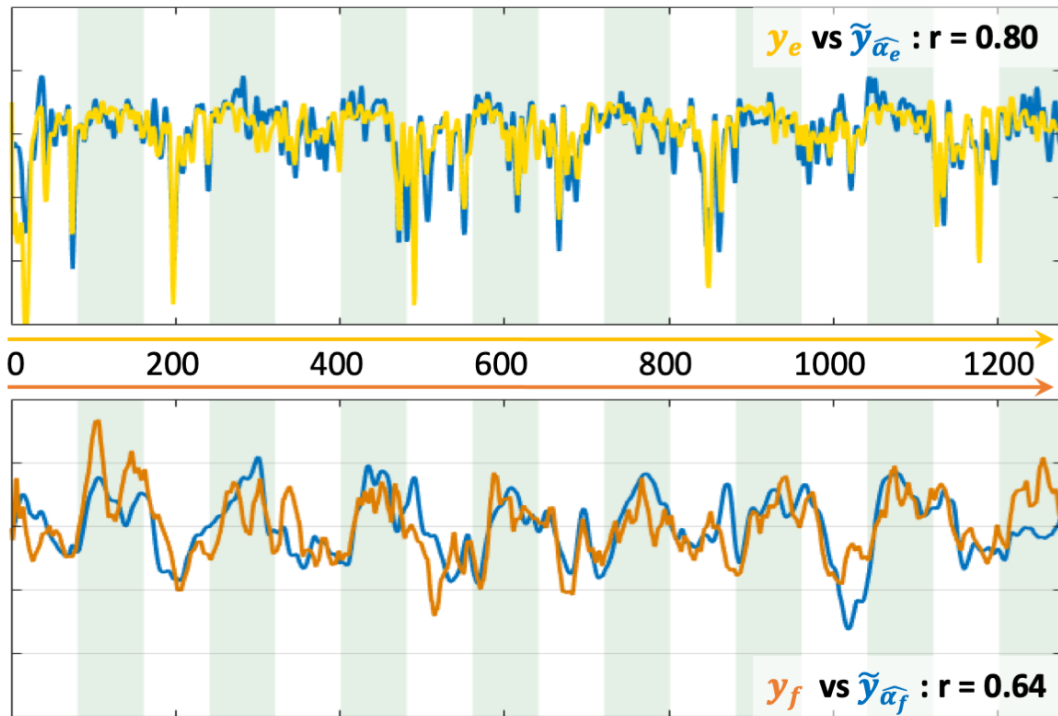


Figure 6. Examples of prediction of NF scores. The x-axis is the temporal axis in milliseconds. Vertical bands indicate the rest and the task blocks. The correlation coefficient r indicates the correlation between each pair of time-series NF scores. Top: the ground truth y_e is in yellow and its estimate in blue. Bottom: the ground truth y_f is in orange and its estimate in blue.

Examples of NF prediction are given at Figure 6, the bottom plot shows the prediction $\tilde{y}_{\hat{\alpha}_f}$ of y_f on a testing set.

To observe the dispersion, over sessions and subjects, of the learned non-zero coefficients, we first denote $\hat{\zeta}_c = \sum_j^{17} \sum_{s_1=1, s_2=1}^3 |\hat{\alpha}_c^{(j, s_1, s_2)}| \in \mathbb{R}^{M \times B}$ the absolute activation pattern, and $\hat{\gamma}_c = \sum_j \sum_{s_1=1, s_2=1}^3 \hat{\alpha}_c^{(j, s_1, s_2)} \in \mathbb{R}^{M \times B}$ the average activation pattern. By construction of the design matrix \mathbf{X}_c , $\hat{\alpha}_c$ can be split into 4 activation patterns, and therefore, we can display heat maps for the 4 absolute activation patterns $\in \{1; \dots; E\}$ (Figure 7, top line) $\sum_{b \in B} \hat{\zeta}_0, \sum_b \hat{\zeta}_3, \sum_b \hat{\zeta}_4$ and $\sum_b \hat{\zeta}_5$; and color maps of the 4 average patterns $\sum_b \hat{\gamma}_0, \sum_b \hat{\gamma}_3, \sum_b \hat{\gamma}_4$ and $\sum_b \hat{\gamma}_5$ showing the sign of the strongest and stable coefficients across subjects and sessions. Interestingly, the most intense heat map, $\sum_b \hat{\zeta}_0$ with a maximum value of 45, concentrates its non-zero values on C3 channel (above the right-hand motor area) and corresponds to the design matrix \mathbf{X}_0 , directly extracted from EEG signal without temporal delay. The next heat map in intensity order is $\sum_b \hat{\zeta}_5$ with two peaks above the visual cortex (Pz and P4 channels). All maps are sparse and present different distributions of the non-zero values. It is also interesting to observe that the main activation peaks (C3, Pz and P4) have opposite signs, suggesting a negative correlation with a delay of 5 seconds between C3 and the posterior Pz, P4. This is not an absurd finding since NF scores are visual, subjects are focused on the visualisation of NF scores during task, and rest during resting blocks

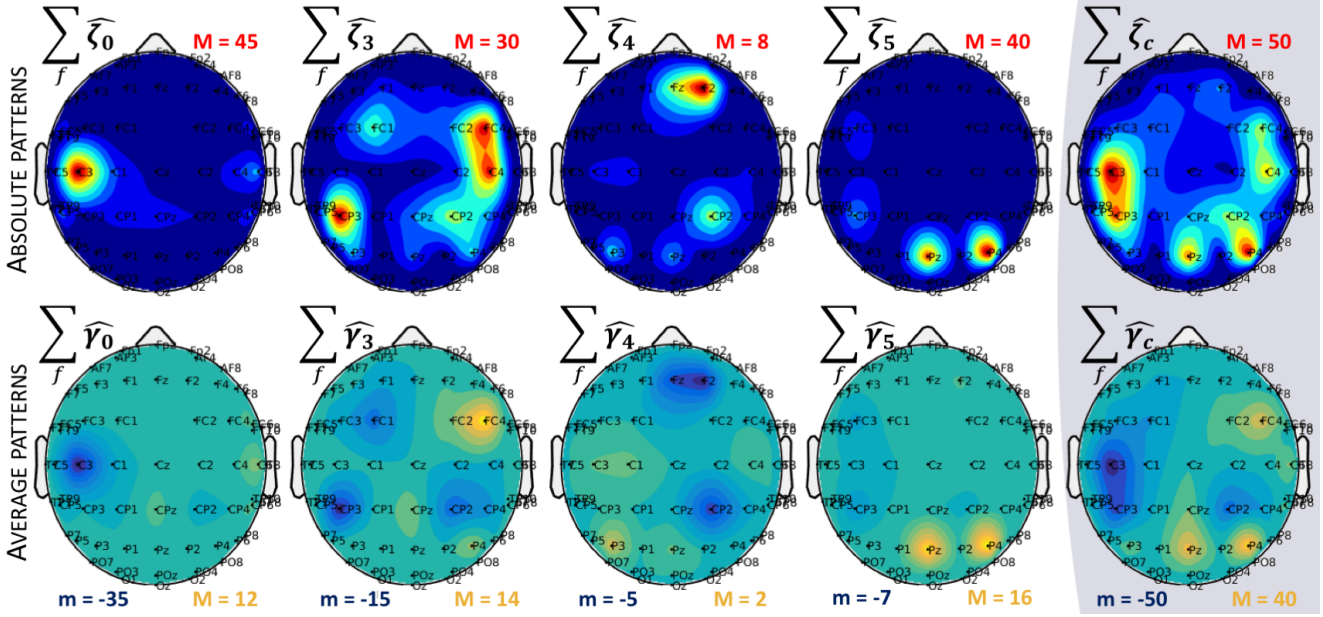


Figure 7. Activation patterns averaged over sessions and subjects. $f \in \{1, \dots, B\}$. Top line: Heat map representing the distribution of non-zero coefficients. Maximum value is indicated for each map with the red letter M. Bottom line: Average activation patterns, representing the sign of the main non-zero values across subject and sessions. Minimum and maximum values are indicated for each map with the letters m and M.

(eyes open). This let think that posterior electrodes could be removed from the active set of the design matrix \mathbf{X}_c .

At last, it is also possible to display the frequency profile of each average activation patterns. The 4 frequency profiles are $\sum_{e \in \{1, \dots, E\}} \hat{\gamma}_0$, $\sum_e \hat{\gamma}_3$, $\sum_e \hat{\gamma}_4$ and $\sum_e \hat{\gamma}_5$, $e \in \{1, \dots, E\}$, summing weights over electrodes. Figure 8 shows that the most used frequency bands over all subjects and sessions are alpha band ([8-12] Hz) and lower beta band ([13-17] Hz), the last 4 frequency bands are not displayed since they only have null coefficients. We can observe the effect of ℓ_2 regularisation which allows continuity in the frequency bands, and the effect of the subsequent ℓ_1 regularisation which removed the smaller coefficients located in the high frequencies. When considering all activation patterns (Figure 8 right side), there is a change of sign between alpha and lower beta. Each activation pattern shows a different frequency profile, which, with Figure 7, tends to demonstrate that all patterns have complementary information.

5 DISCUSSION AND CONCLUSION

The model validation supports that the optimisation strategy we chose for our problem is adapted to the model, as is the choice of the different design matrices. The evaluation of the model prediction suggests that predicting only NF-fMRI scores while applying a Laplacian on EEG signal appears to be the best solution. Indeed, the variability between EEG signals induces decreasing correlation with the reference

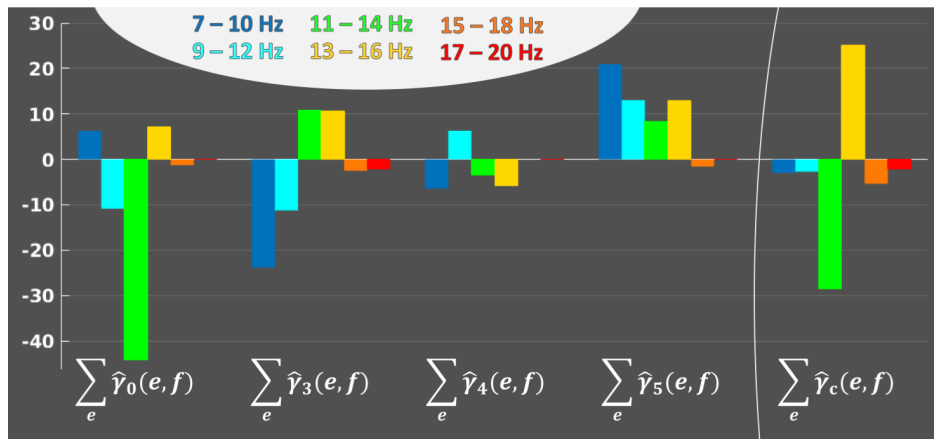


Figure 8. Frequency profiles, across subjects and sessions, of each average activation patterns, to represent the implication of each frequency bands in the activation patterns. $e \in \{1, \dots, E\}$. For each average activation pattern, the y-axis indicates the sum of weights over electrodes, for each frequency bands $f \in \{1, \dots, B\}$ on the horizontal axis.

NF score y_c , for $\tilde{y}_{\hat{\alpha}_c}$ (NF-predictor 1) and for $\tilde{y}_{\hat{\alpha}_e} + \tilde{y}_{\hat{\alpha}_f}$ (NF-predictor 4). Also, when considering the final objective of the proposed model (Figure 1), predicting NF-EEG scores from EEG is not really relevant (except from a pure methodological point of view) since these scores can always be computed from the available EEG signal. However, one might want to improve the selection of features for the computation of NF-EEG scores, but this raises different questions about the validation and the reference score. Here we assumed that the given NF scores are relevant to the task and good enough to be considered as reference scores. It is also interesting to note that for NF-predictor 1, when decomposing the activation pattern $\hat{\alpha}_c$ (from $\tilde{y}_{\hat{\alpha}_c}$), into the 4 matrices corresponding to the different design matrices, the weights corresponding to X_0 (0 second of delay) are mainly located above C3, which is the centre of the Laplacian for the computation of the NF-EEG scores. This seem to support the fact that with a delay of 0 seconds, only the part of the NF coming from the EEG brings information. Information from the fMRI arrives later with a delay, between 3 and 5 seconds here.

Figure 7 and 8 show that only specific electrodes and frequency band (between 7 Hz and 20 Hz, higher frequencies are not selected by the model) are required, over all subjects, letting think that there is a common underlying model for the population, even if models are subject specific.

A possibility to increase the prediction of NF scores, would be to use more NF sessions as learning sessions, since as observed, EEG signals bring variability in the prediction. Each new bi-modal neurofeedback session could be added to the subject-specific model, to better adapt the model to the subject or patient. This will be investigated in a next study.

Presently, the proposed model finds an individual or specific model for each subject that can be seen as a personalised model for neurofeedback sessions. However, for a future work, we are investigating

an adaptation of the methodology for the extraction of a common model, taking into account the differences between subjects, allowing the prediction of NF-EEG-fMRI scores on new subjects who did not participated to the model construction. The model might be less specific, but this would give access to neurofeedback sessions of quality using EEG only, for subjects with MRI contraindications, and/or drive a subject-specific model estimation, respecting the strategy used by the subject to progress in its neurofeedback task.

Other ways to improve the method proposed here would be to investigate the use of dynamic functional connectivity, a relatively recent field in BOLD fMRI which needs further investigations to be used along with EEG data (Tagliazucchi and Laufs, 2015). Dynamic functional connectivity study the temporal fluctuations of the BOLD signal across the brain, and appears to be a promising approach in the EEG-fMRI research field (Allen et al., 2018).

The long-term objective of our project is to learn from EEG-fMRI NF sessions to provide, outside the MRI scanner, better NF-EEG sessions (Figure 1). A future work will investigate the portability of the learned model (on EEG-fMRI neurofeedback data), outside the MRI scanner, bringing new challenges as dealing with the remaining noises in the MRI after artefact correction, and the absence of ground truth once the EEG is measured outside the MRI.

To conclude, the 5th NF-predictor proposed here is able to provide a good enough prediction of the NF-fMRI scores, to overcome the absence of NF-fMRI and allows to significantly increase the quality of the estimation of NF-EEG-fMRI scores when using EEG only.

6 AUTHOR CONTRIBUTIONS

CC guarantor of integrity of entire study. Study concepts and design, data analysis and interpretation, all authors; manuscript drafting or manuscript revision for important intellectual content, all authors; approval of final version of submitted manuscript, all authors.

7 CONFLICT OF INTEREST STATEMENT

The authors declare that the research was conducted in the absence of any commercial or financial relationships that could be construed as a potential conflict of interest.

8 ACKNOWLEDGEMENTS

Data acquisition was supported by the Neurinfo MRI research facility from the University of Rennes I. Neurinfo is granted by the the European Union (FEDER), the French State, the Brittany Council,

Rennes Metropole, Inria, Inserm and the University Hospital of Rennes. This work has received a French government support granted to the CominLabs excellence laboratory and managed by the National Research Agency in the “Investissements d’Avenir” program under reference ANR-10-LABX-07-01. It was also funded by Brittany region under HEMISFER project.

REFERENCES

- Abreu, R., Leal, A., and Figueiredo, P. (2018). EEG-Informed fMRI: A Review of Data Analysis Methods. *Frontiers in Human Neuroscience* 12
- Allen, E. A., Damaraju, E., Eichele, T., Wu, L., and Calhoun, V. D. (2018). EEG Signatures of Dynamic Functional Network Connectivity States. *Brain Topography* 31, 101–116
- Beck, A. and Teboulle, M. (2009). A Fast Iterative Shrinkage-Thresholding Algorithm for Linear Inverse Problems. *SIAM Journal on Imaging Sciences* 2, 183–202
- Birbaumer, N., Ramos Murguialday, A., Weber, C., and Montoya, P. (2009). Chapter 8 Neurofeedback and Brain–Computer Interface. In *International Review of Neurobiology* (Elsevier), vol. 86. 107–117
- Combettes, P. L. and Wajs, V. R. (2005). Signal Recovery by Proximal Forward-Backward Splitting. *Multiscale Modeling & Simulation* 4, 1168–1200
- de Munck, J., Gonçalves, S., Huijboom, L., Kuijer, J., Pouwels, P., Heethaar, R., et al. (2007). The hemodynamic response of the alpha rhythm: An EEG/fMRI study. *NeuroImage* 35, 1142–1151
- de Munck, J., Gonçalves, S., Mammoliti, R., Heethaar, R., and Lopes da Silva, F. (2009). Interactions between different EEG frequency bands and their effect on alpha–fMRI correlations. *NeuroImage* 47, 69–76
- Engell, A. D., Huettel, S., and McCarthy, G. (2012). The fMRI BOLD signal tracks electrophysiological spectral perturbations, not event-related potentials. *NeuroImage* 59, 2600–2606. doi:10.1016/j.neuroimage.2011.08.079
- Formaggio, E., Storti, S. F., Bertoldo, A., Manganotti, P., Fiaschi, A., and Toffolo, G. M. (2011). Integrating EEG and fMRI in epilepsy. *NeuroImage* 54, 2719–2731
- Friston, K. J., Jezzard, P., and Turner, R. (1994). Analysis of functional MRI time-series. *Human Brain Mapping* 1, 153–171
- Goncalves, S. I., Bijma, F., Pouwels, P. W. J., Jonker, M., Kuijer, J. P. A., Heethaar, R. M., et al. (2008). A Data and Model-Driven Approach to Explore Inter-Subject Variability of Resting-State Brain Activity Using EEG-fMRI. *IEEE Journal of Selected Topics in Signal Processing* 2, 944–953
- Gramfort, A., Kowalski, M., and Hämäläinen, M. (2012). Mixed-norm estimates for the M/EEG inverse problem using accelerated gradient methods. *Physics in Medicine and Biology* 57, 1937–1961

- Gramfort, A., Strohmeier, D., Haueisen, J., Hamalainen, M., and Kowalski, M. (2011). Functional Brain Imaging with M/EEG Using Structured Sparsity in Time-Frequency Dictionaries. In *IPMI*, eds. G. Székely and H. K. Hahn (Berlin, Heidelberg: Springer Berlin Heidelberg), vol. 6801. 600–611
- Grech, R., Cassar, T., Muscat, J., Camilleri, K. P., Fabri, S. G., Zervakis, M., et al. (2008). Review on solving the inverse problem in EEG source analysis. *Journal of NeuroEngineering and Rehabilitation* 5, 25. doi:10.1186/1743-0003-5-25
- Hammond, D. C. (2011). What is Neurofeedback: An Update. *Journal of Neurotherapy* 15, 305–336
- Handwerker, D. A., Ollinger, J. M., and D’Esposito, M. (2004). Variation of BOLD hemodynamic responses across subjects and brain regions and their effects on statistical analyses. *NeuroImage* 21, 1639–1651
- Leite, M., Leal, A., and Figueiredo, P. (2013). Transfer Function between EEG and BOLD Signals of Epileptic Activity. *Frontiers in Neurology* 4
- Lindquist, M. A., Meng Loh, J., Atlas, L. Y., and Wager, T. D. (2009). Modeling the hemodynamic response function in fMRI: Efficiency, bias and mis-modeling. *NeuroImage* 45, S187–S198
- Logothetis, N. K., Pauls, J., Augath, M., Trinath, T., and Oeltermann, A. (2001). Neurophysiological investigation of the basis of the fMRI signal. *Nature* 412, 150–157. doi:10.1038/35084005
- Magri, C., Schridde, U., Murayama, Y., Panzeri, S., and Logothetis, N. K. (2012). The Amplitude and Timing of the BOLD Signal Reflects the Relationship between Local Field Potential Power at Different Frequencies. *Journal of Neuroscience* 32, 1395–1407. doi:10.1523/JNEUROSCI.3985-11.2012
- Mano, M., Lécuyer, A., Bannier, E., Perronnet, L., Noorzadeh, S., and Barillot, C. (2017). How to Build a Hybrid Neurofeedback Platform Combining EEG and fMRI. *Frontiers in Neuroscience* 11
- Meir-Hasson, Y., Kinreich, S., Podlipsky, I., Hendler, T., and Intrator, N. (2014). An EEG Finger-Print of fMRI deep regional activation. *NeuroImage* 102, 128–141
- Moosmann, M., Eichele, T., Nordby, H., Hugdahl, K., and Calhoun, V. D. (2008). Joint independent component analysis for simultaneous EEG–fMRI: Principle and simulation. *International Journal of Psychophysiology* 67, 212–221. doi:10.1016/j.ijpsycho.2007.05.016
- Noorzadeh, S., Maurel, P., Oberlin, T., Gribonval, R., and Barillot, C. (2017). Multi-modal EEG and fMRI Source Estimation Using Sparse Constraints. In *Medical Image Computing and Computer Assisted Intervention MICCAI 2017*, eds. M. Descoteaux, L. Maier-Hein, A. Franz, P. Jannin, D. L. Collins, and S. Duchesne (Cham: Springer International Publishing), vol. 10433. 442–450
- Ou, W., Hämäläinen, M. S., and Golland, P. (2009). A distributed spatio-temporal EEG/MEG inverse solver. *NeuroImage* 44, 932–946

- Pedregosa, F., Eickenberg, M., Thirion, B., and Gramfort, A. (2013). HRF Estimation Improves Sensitivity of fMRI Encoding and Decoding Models. In *2013 International Workshop on Pattern Recognition in Neuroimaging* (Philadelphia, PA, USA: IEEE), 165–169
- Perronnet, L., Lécuyer, A., Mano, M., Bannier, E., Lotte, F., Clerc, M., et al. (2017). Unimodal Versus Bimodal EEG-fMRI Neurofeedback of a Motor Imagery Task. *Frontiers in Human Neuroscience* 11
- Perronnet, L., Lécuyer, A., Mano, M., Clerc, M., Lotte, F., and Barillot, C. (2018). Learning 2-in-1: towards integrated EEG-fMRI-neurofeedback. *bioRxiv*
- Ramoser, H., Müller-gerking, J., and Pfurtscheller, G. (2000). Optimal spatial filtering of single trial EEG during imagined hand movement. *IEEE Trans. Rehabil. Eng.*, 441–446
- Rosa, M. J., Kilner, J., Blankenburg, F., Josephs, O., and Penny, W. (2010). Estimating the transfer function from neuronal activity to BOLD using simultaneous EEG-fMRI. *NeuroImage* 49, 1496–1509
- Scheeringa, R., Fries, P., Petersson, K.-M., Oostenveld, R., Grothe, I., Norris, D. G., et al. (2011). Neuronal Dynamics Underlying High- and Low-Frequency EEG Oscillations Contribute Independently to the Human BOLD Signal. *Neuron* 69, 572–583. doi:10.1016/j.neuron.2010.11.044
- Schwab, S., Koenig, T., Morishima, Y., Dierks, T., Federspiel, A., and Jann, K. (2015). Discovering frequency sensitive thalamic nuclei from EEG microstate informed resting state fMRI. *NeuroImage* 118, 368–375
- Siero, J. C., Hermes, D., Hoogduin, H., Luijten, P. R., Petridou, N., and Ramsey, N. F. (2013). BOLD Consistently Matches Electrophysiology in Human Sensorimotor Cortex at Increasing Movement Rates: A Combined 7t fMRI and ECoG Study on Neurovascular Coupling. *Journal of Cerebral Blood Flow & Metabolism* 33, 1448–1456. doi:10.1038/jcbfm.2013.97
- Sulzer, J., Haller, S., Scharnowski, F., Weiskopf, N., Birbaumer, N., Blefari, M., et al. (2013). Real time fMRI neurofeedback: Progress and challenges. *NeuroImage* 76, 386–399. doi:10.1016/j.neuroimage.2013.03.033
- Tagliazucchi, E. and Laufs, H. (2015). Multimodal Imaging of Dynamic Functional Connectivity. *Frontiers in Neurology* 6
- Thibault, R. T., MacPherson, A., Lifshitz, M., Roth, R. R., and Raz, A. (2018). Neurofeedback with fMRI: A critical systematic review. *NeuroImage* 172, 786–807
- Wang, T., Mantini, D., and Gillebert, C. R. (2017). The potential of real-time fMRI neurofeedback for stroke rehabilitation: A systematic review. *Cortex* doi:10.1016/j.cortex.2017.09.006
- Zotev, V., Phillips, R., Yuan, H., Misaki, M., and Bodurka, J. (2014). Self-regulation of human brain activity using simultaneous real-time fMRI and EEG neurofeedback. *NeuroImage* 85, 985–995. doi:10.1016/j.neuroimage.2013.04.126